Full Paper
doi.org/10.1002/chem.202000297

High-pressure Chemistry | *Hot Paper*

$Sr_3P_3N_7$: Complementary Approach by Ammonothermal and High-Pressure Syntheses

Mathias Mallmann[+],[a] Sebastian Wendl[+],[a] Philipp Strobel,[b] Peter J. Schmidt,[b] and Wolfgang Schnick*[a]

Abstract: Nitridophosphates exhibit an intriguing structural diversity with different structural motifs, for example, chains, layers or frameworks. In this contribution the novel nitridophosphate $Sr_3P_3N_7$ with unprecedented *dreier* double chains is presented. Crystalline powders were synthesized using the ammonothermal method, while single crystals were obtained by a high-pressure multianvil technique. The crystal structure of $Sr_3P_3N_7$ was solved and refined from single-crystal X-ray diffraction and confirmed by powder X-ray methods. $Sr_3P_3N_7$ crystallizes in monoclinic space group *P*2/*c*. Energy-dispersive X-ray and Fourier-transformed infrared spectroscopy were conducted to confirm the chemical composition, as well as the absence of NH_x functionality. The optical band gap was estimated to be 4.4 eV using diffuse reflectance UV/Vis spectroscopy. Upon doping with Eu^{2+}, $Sr_3P_3N_7$ shows a broad deep-red to infrared emission (λ_{em} = 681 nm, fwhm ≈ 3402 cm^{-1}) with an internal quantum efficiency of 42 %.

Introduction

Due to the fact that the element combination P/N is isoelectronic to Si/O, nitridophosphates exhibit structural analogies to silicates and are built up from condensed or non-condensed PN_4 tetrahedra. In recent years, numerous nitridophosphates have been synthesized with a high structural diversity with different degrees of condensation κ (ratio of tetrahedra centres to ligands) ranging from 1/4 to 4/7.[1] Thereby, different structural motifs like non-condensed tetrahedra, chains, layers or frameworks can occur.[2–5] Particularly due to their structural diversity, these compounds exhibit diverse, interesting physical properties, for example luminescence upon doping with Eu^{2+}. So far, P/N-network and -layer compounds such as MP_2N_4 (*M* = Ca, Sr, Ba), $Ba_3P_5N_{10}X$ (*X* = Cl, Br, I) or $BaP_6N_{10}NH$ were used as host lattices, covering emission in almost the entire visible spectrum.[6–9] Especially, $Ba_3P_5N_{10}Br$, crystallizing in a zeolite-like structure, exhibits intriguing luminescence properties and is discussed as a natural-white-light single emitter, demonstrating nicely the potential of nitridophosphate materials.[7]

But in contrast to silicates, only a few nitridophosphates could be synthesized under ambient pressure conditions (e.g., Ca_2PN_3, $Li_{10}P_4N_{10}$).[3,10,11] This is due to the fact that the appropriate temperature range for crystallization of nitridophosphates is significantly beyond the decomposition temperature of the most important starting material P_3N_5, which can be circumvented by applying high-pressure methods.

Among these, the multianvil approach is the most frequently employed method, following Le Chatelier's principle in order to compensate thermal decomposition. Over the years, different synthesis strategies using the multianvil approach were developed, including the azide route, high-pressure metathesis or the synthesis with ammonium chloride as mineralizer.[5,6,12] The most valuable advantage of this technique is that the enormous pressure allows for sufficient temperatures for the reconstructive cleavage of P–N bonds. Furthermore, in many cases these high temperatures enable the formation of single crystals, facilitating structure elucidation significantly. However, a drawback of such high-pressure methods is the low sample volume, especially in the context of materials characterization and application.

Therefore, a promising alternative for nitridophosphate synthesis is the ammonothermal approach as a medium pressure method. Herein, the reduced pressure, compared to the multianvil technique, is compensated by the usage of a highly reactive supercritical ammonia atmosphere. In 1997 Jacobs and coworkers used this approach to synthesize $K_3P_6N_{11}$.[13] In the meantime, the ammonothermal method enabled synthesis of nitridophosphates with isolated tetrahedra units, chains, layers

[a] *M. Mallmann,[+] S. Wendl,[+] Prof. Dr. W. Schnick*
Department of Chemistry
University of Munich (LMU)
Butenandtstraße 5–13 (D), 81377 Munich (Germany)
E-mail: wolfgang.schnick@uni-muenchen.de

[b] *Dr. P. Strobel, Dr. P. J. Schmidt*
Lumileds Phosphor Center Aachen
Lumileds (Germany) GmbH
Philipsstraße 8, 52068 Aachen (Germany)

[+] *These authors contributed equally to this work.*

Supporting information and the ORCID identification number(s) for the author(s) of this article can be found under: https://doi.org/10.1002/chem.202000297.

and frameworks.[14,15] Even nitridophosphates like SrP_8N_{14} or $Li_{18}P_6N_{16}$, which were so far only accessible by the high-pressure multianvil approach, could be synthesized under ammonothermal conditions in high yield, simplifying the investigation of their physical properties significantly. Although, the ammonothermal method was already used for synthesis of numerous nitride materials,[16–22] the crystal growth of ternary or quaternary nitrides during ammonothermal synthesis, except for a few examples like Mg_2PN_3 or $MTaN_2$ (M = Na, K, Rb, Cs), is still challenging.[15,23]

In this contribution, we present a combination of medium- and high-pressure methods with their respective advantages for the investigation of unknown nitridophosphates. We report on $Sr_3P_3N_7$ as a case study for a complementary approach of ammonothermal and multianvil syntheses. $Sr_3P_3N_7$ extends the class of ternary alkaline earth nitridophosphates by the degree of condensation of $\kappa = 3/7$. Structure elucidation was based on single-crystal X-ray diffraction data, enabled by high-pressure synthesis, while ammonothermal methods facilitated bulk synthesis for further analysis, as well as studies on the luminescence properties of $Sr_3P_3N_7$:Eu^{2+}.

Results and Discussion

Synthesis

The title compound initially has been observed in heterogeneous products obtained by ammonothermal as well as high-pressure methods, targeting new nitridophosphates with a low degree of condensation. While high-pressure high-temperature synthesis leads to suitable single crystals for structure elucidation, ammonothermal synthesis provided the highest yield of bulk samples, expressing the complementary approach. The synthesis of single crystals was started from stoichiometric amounts of $Sr(N_3)_2$ and P_3N_5 according to Equation 1 together with small amounts of $EuCl_2$. The starting mixture was treated by high-pressure high-temperature reaction at 5 GPa and 1270 K. These reaction conditions were achieved by using a hydraulic 1000 t press and a modified Walker-type multianvil apparatus.[24,25]

$$3\,Sr(N_3)_2 + P_3N_5 \rightarrow Sr_3P_3N_7 + 8\,N_2 \qquad (1)$$

Analogously, translucent orange $Sr_3P_3N_7$:Eu^{2+} crystals of up to 40 μm in length were isolated (see Scanning electron microscopy section). After optimizing the synthesis based on the results of single-crystal X-ray diffraction and energy dispersive X-ray spectroscopy, bulk samples of $Sr_3P_3N_7$ were prepared under ammonothermal conditions in custom-built high-temperature autoclaves using SrH_2, P_3N_5 and the ammonobasic mineralizer NaN_3. NaN_3 decomposes at elevated temperatures and forms $NaNH_2$ in situ, which increases the solubility of the other starting materials by formation of intermediate species (e.g., $Na_2Sr_3(NH_2)_8$, $Na_{10}[P_4(NH)_6]N_4(NH_2)_6(NH_3)_{0.5}$ or $P_3N_3(NH_2)_6$) which have already been observed under ammonothermal conditions at temperatures around 670 K.[26–28] Subsequent heating to 1070 K, reaching a maximum pressure of 140 MPa in the autoclave, resulted in synthesis of $Sr_3P_3N_7$ as a crystalline white powder, which hydrolyses slowly on exposure to moist air. The product was therefore washed with dry ethanol to remove residual mineralizer and intermediate species. Analogous syntheses with red phosphorus instead of P_3N_5 also resulted in the desired product. Doping with Eu^{2+} (nominal concentration of 2 mole% with respect to Sr) in the form of $Eu(NH_2)_2$ resulted in deep-red luminescence of $Sr_3P_3N_7$:Eu^{2+} when irradiated with UV light (see Luminescence section).

Crystal structure

The crystal structure of $Sr_3P_3N_7$ was solved and refined from single-crystal X-ray diffraction data in monoclinic space group $P2/c$ (no. 13). Details on the structure determination are summarized in Table 1. Atomic coordinates and anisotropic displacement parameters are given in Table S1 and S2 in the Supporting Information. Selected interatomic distances and bond angles are summarized in the Supporting Information (Table S3). With $\kappa = n(P)/n(N) = 3/7$, $Sr_3P_3N_7$ has a hitherto unknown degree of condensation of an alkaline earth nitridophosphate and is composed of infinite PN_4-tetrahedra *dreier* double chains. A degree of condensation of $\kappa = 3/7$ is already known for rare earth nitridophosphates ($RE_2P_3N_7$ with RE = La, Ce, Pr, Nd, Sm, Eu, Ho, Yb), however, there is no structural correlation between these compounds.[29] Apart from Ca_2PN_3, $Sr_3P_3N_7$ is the only known alkaline earth nitridophosphate with a chain structure, while Mg_2PN_3 crystallizes strictly speaking in a wurtzite-type superstructure and can be interpreted as a

Table 1. Crystallographic data of $Sr_3P_3N_7$ (synthesized by the multianvil approach) obtained from single-crystal X-ray diffraction.

Formula	$Sr_3P_3N_7$
crystal system	monoclinic
space group	$P2/c$ (no. 13)
lattice parameters [Å,°]	$a = 6.882(8)$
	$b = 7.416(9)$
	$c = 7.036(8)$
	$\beta = 104.96(3)$
cell volume [Å^3]	346.9(7)
formula units / cell	2
Density [g cm^{-3}]	4.345
crystal size [mm]	0.02 × 0.02 × 0.03
μ [mm^{-1}]	23.617
T [K]	298(2)
Diffractometer	Bruker D8 Quest
radiation (λ [Å])	$Mo_{K\alpha}$ (0.71073)
F (000)	416
θ range [°]	2.7–30.5
total no. of reflections	3621
no. of independent reflections	1064
observed reflections ($F^2 > 2\sigma(F^2)$)	728
R_{int}; R_σ	0.0858; 0.0970
structure solution	SHELXT
structure refinement	SHELXL-97
refined parameters	61
goodness of fit (χ^2)	1.044
$R1$ (all data); $R1$ ($F^2 > 2\sigma(F^2)$)	0.100; 0.059
$wR2$ (all data); $wR2$ ($F^2 > 2\sigma(F^2)$)	0.131; 0.117
$\Delta\rho_{max}$; $\Delta\rho_{min}$ [e Å^{-3}]	1.892, −1.790

double nitride.[3,30] The chains in $Sr_3P_3N_7$ show a periodicity of $P=3$ and a stretching factor of $f_c=0.90$ (see Figure 1) and are built up from *dreier*-rings according to Liebau.[31,32] Two of these *dreier*-rings, which are structurally related to each other by a rotating mirror axis (2/*m*), are connected through two common corners forming an additional *vierer*-ring. The resulting $[P_6N_{16}]$-units were already found in $Li_{18}P_6N_{16}$ as non-condensed $[P_6N_{16}]^{18-}$ anions.[14,33] In the title compound these subunits are connected by two common corners on each side, forming infinite chains. The P–N distances vary from 1.575 to 1.683 Å. As expected, the shortest distances belong to the terminal P(2)–N(2) atoms. The corresponding N-P-N bond angles are between 103.3(5) and 115.0(4)°. Angles as well as distances are in good agreement with values observed in other nitridophosphates described in literature.[3,4,13,29]

The infinite chains are oriented along [0 0 1] and are stacked congruently in *a* and *b* (see Figure 2). The crystal structure contains two crystallographically different Sr sites. The Sr1 site is located between two chains stacked along [1 0 0] and is coordinated by 10 N atoms with distances between 2.740(9) and 3.068(10) Å. In contrast, the second Sr site (Sr2) is located between two chains stacked along [0 1 0] and is coordinated by 9 N atoms with distances ranging from 2.504(10) to 3.283(10) Å. The coordination polyhedra of both sites are illustrated in Figure S1 in the Supporting Information. All Sr–N distances are in good agreement with values from other Sr (oxo)-nitridophosphates known from literature (e.g., SrP_2N_4, SrP_3N_5O, $Sr_3P_6O_6N_8$).[34–36]

To confirm the structure model obtained from single-crystal X-ray data, a PXRD measurement and subsequent Rietveld refinement were conducted (Figure 3). The refined crystallographic data, as well as Wyckoff positions, are summarized in Table S4 and S5 in the Supporting Information. As described above (Synthesis section), residual mineralizer ($NaNH_2$) can be removed by washing with dry ethanol. However, the sample partially decomposes during the washing process, resulting in the formation of an amorphous side-phase. Due to this fact, the unwashed sample was used for Rietveld refinement. A comparison of washed and unwashed samples is illustrated in Figure S2 in the Supporting Information.

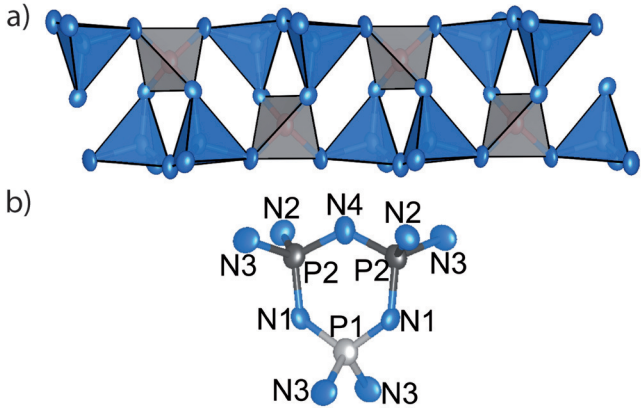

Figure 1. Infinite *dreier* double chain (a) and *dreier*-ring subunit (b). Thermal ellipsoids are depicted at 90% probability.

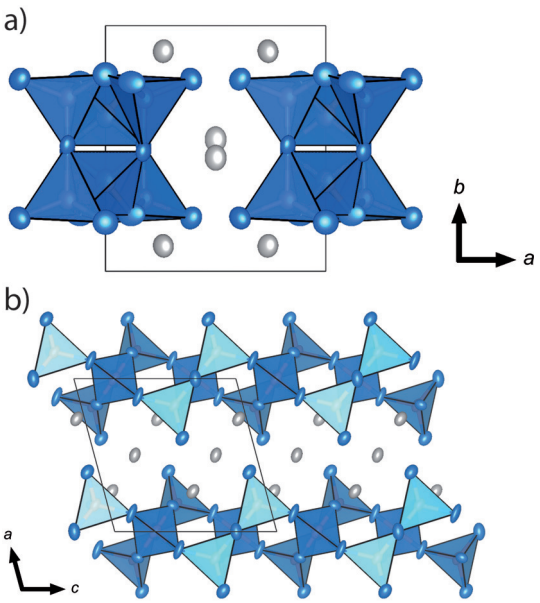

Figure 2. Crystal structure of $Sr_3P_3N_7$ viewed along [0 0 1] (a) and [0 1 0] (b). PN_4 tetrahedra and N atoms are depicted in blue, Sr atoms in grey. Thermal ellipsoids are depicted at 90% probability.

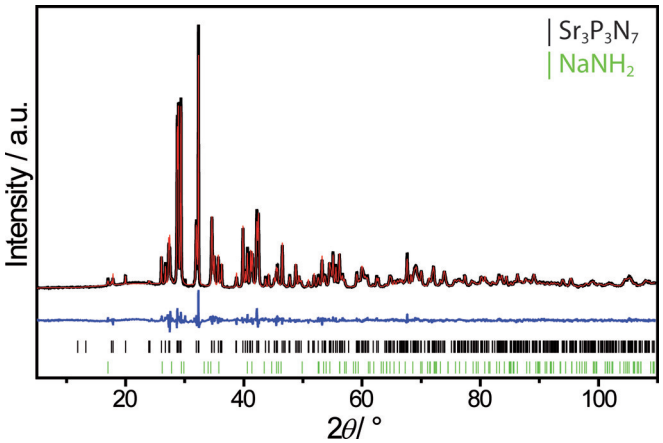

Figure 3. Rietveld refinement of PXRD measurements of ammonothermally synthesized $Sr_3P_3N_7$ with experimental data (black line), calculated data (red line), difference profile (blue line) and reflection positions ($Sr_3P_3N_7$: black bars, $NaNH_2$: green bars).

Scanning electron microscopy

Energy dispersive X-ray (EDX) spectroscopy was used for determination of the chemical composition. The determined atomic ratios are in good agreement with the expected chemical formulas (see Table S5 in the Supporting Information). Traces of europium can be attributed to doping of the sample and oxygen impurities to surface hydrolysis of the products. Furthermore, a scanning electron micrograph of the product was collected and is illustrated in Figure 4.

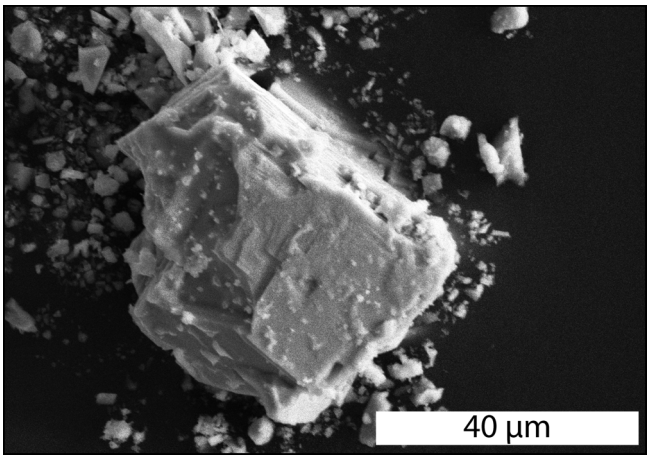

Figure 4. SEM image of a $Sr_3P_3N_7$ single crystal obtained from high-pressure synthesis.

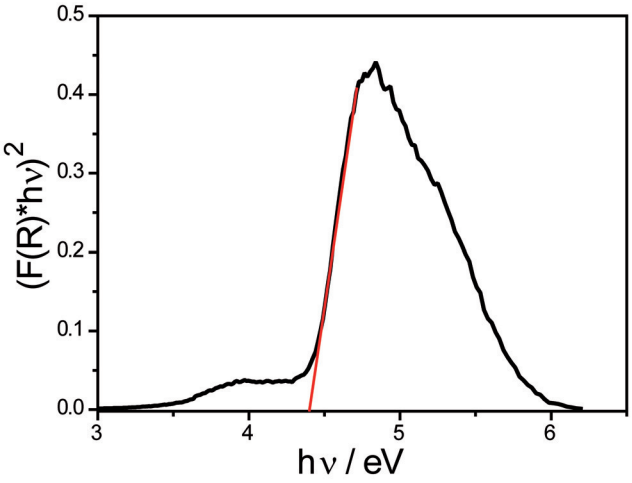

Figure 5. Tauc plot (black line) of ammonothermally synthesized $Sr_3P_3N_7$. Red line as a tangent at the inflection point.

Fourier Transform Infrared spectroscopy

A FTIR spectrum was recorded in order to prove the absence of any NH_x functionality in $Sr_3P_3N_7$. The spectrum (see Figure S3 in the Supporting Information) shows no significant absorption bands around 3000 cm^{-1}, indicating the absence of N–H groups in accordance to the crystal structure obtained from single-crystal X-ray diffraction, since the presence of imide or amide groups would lead to strong absorption bands.[4] Weak signals could be attributed to partial surface hydrolysis of the products. The absorption bands between 500 and 1300 cm^{-1} can be attributed to symmetric and asymmetric stretching modes of the P-N-framework and are characteristic for nitridophosphates.

UV/Vis spectroscopy

Diffuse reflectance UV/Vis spectroscopy was conducted to estimate the optical band gap of the undoped sample. Therefore, the Kubelka–Munk function $F(R)=(1-R)^2/2R$ was used to convert the measured diffuse reflectance spectrum to a pseudo-absorption spectrum.[37] A Tauc plot (see Figure 5) was then used to estimate the optical band gap by plotting $(F(R)\cdot h\nu)^{1/n}$ versus $h\nu$ (with $n=1/2$, assuming direct transition) and drawing of a tangent at the inflection point.[38] The diffuse reflectance spectrum shows an absorption band around 250 nm (see Figure S4 in the Supporting Information). The determined band gap is approximately 4.4 eV.

A diffuse reflectance spectrum of the Eu^{2+} doped sample is illustrated in Figure S5. It shows an additional broad absorption band between 400 and 550 nm, which can be attributed to dopant absorption and is in good agreement with the corresponding excitation spectrum (see Luminescence section).

Luminescence

Luminescence properties of $Sr_3P_3N_7:Eu^{2+}$ were measured from crystalline powder samples. $Sr_3P_3N_7:Eu^{2+}$ shows deep-red luminescence when irradiated with UV to blue light (see Figure S6 in the Supporting Information). The emission spectrum ($\lambda_{exc}=$ 450 nm) and the excitation spectrum are illustrated in Figure 6. The excitation spectrum has two maxima at around 405 and 465 nm, while the emission spectrum (2 mole% Eu with respect to Sr) shows one broad band in the deep-red to infrared region ($\lambda_{em}=681$ nm) with a full width at half maximum (fwhm) of 162 nm/3402 cm^{-1}. The broad emission band probably results from the different coordination of the cations (see Crystal structure section). In order to capture the complete emission spectrum, a second spectrometer was used for the measurement ($\lambda_{exc}=410$ nm) of the emission in the IR region beyond 800 nm. This leads to the higher background level above 800 nm. The internal quantum efficiency (IQE) was determined with an excitation wavelength of 438 nm to be 42% in the range up to 800 nm. These luminescent properties make $Sr_3P_3N_7:Eu^{2+}$ interesting, as such materials may be applied in horticultural lighting, as they can convert green light into the red to IR spectral range with increased photosynthesis quantum efficiency. A further possible application field is, for example, hyper- or multispectral imaging, with diverse applications in for example, agriculture, automated driving or molecular biology.[39,40]

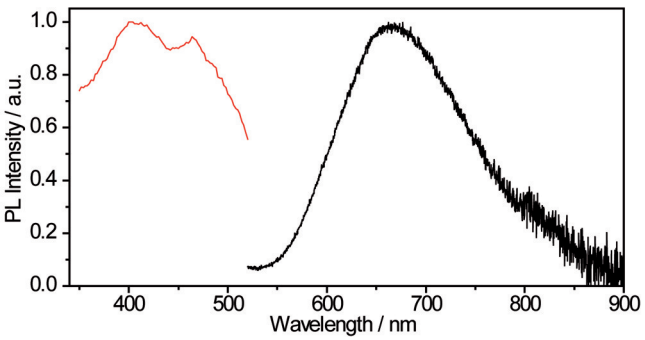

Figure 6. Excitation (red line) and emission (black line) spectra of ammonothermally synthesized $Sr_3P_3N_7:Eu^{2+}$.

Conclusions

In this contribution we present a complementary approach of ammonothermal and multianvil techniques as a powerful combination for a simplified and much faster access to a detailed structural and physical analysis of nitridophosphates. Exploitation of the advantages of each method led to the discovery of the new nitridophosphate $Sr_3P_3N_7$. Thereby, the best crystallization conditions were realized via a high-pressure approach using the azide route, allowing higher temperatures during syntheses compared to the ammonothermal approach. The structure model was solved and refined from single-crystal X-ray diffraction data. $Sr_3P_3N_7$ is composed of unprecedented *dreier* double chains made up of PN_4 tetrahedra with a degree of condensation $\kappa = 3/7$, which is hitherto unknown for alkaline earth nitridophosphates. Due to larger sample volumes, studies on the physical properties of the title compound were carried out with bulk samples obtained from ammonothermal synthesis. The band gap (4.4 eV) was determined using diffuse reflectance spectroscopy. Upon doping with Eu^{2+}, $Sr_3P_3N_7$ exhibits a broad emission band in the deep-red to infrared region ($\lambda_{em} =$ 681 nm, fwhm $\approx$ 3402 cm^{-1}) with an internal quantum efficiency of 42%, making it practically interesting for commercial applications (e.g., horticultural lighting). For this purpose, stoichiometry and doping concentration optimization as major parts of an industrial process development will further improve the luminescence efficiency.

Experimental Section

All manipulations were conducted in argon-filled gloveboxes (Unilab, MBraun, Garching, $O_2 < 1$ ppm, $H_2O < 1$ ppm) under exclusion from oxygen and moisture because of the air sensitivity of starting materials and products. A vacuum line (≤ 0.1 Pa) with argon and ammonia (both: Air Liquide, 99.999%) supply was used for filling of the autoclaves with NH_3. The gases were further purified by gas cartridges (Micro torr FT400-902 (for Ar) and MC400-702FV (for NH_3), SAES Pure Gas Inc., San Luis Obispo, CA, USA), providing a purity level of <1 ppbV H_2O, O_2 and CO_2.

Synthesis of $Eu(NH_2)_2$: $Eu(NH_2)_2$ was synthesized ammonothermally starting from Eu metal (99.99%, smart elements). The experiment was carried out analogously to the synthesis described in literature.[41]

Synthesis of P_3N_5: P_3N_5 was synthesized following Stock et al.[42] by ammonolysis of P_4S_{10} (Sigma Aldrich, 99%) at 1125 K for 4 h (heating rate: 5 K min^{-1}). Before reaction, the silica tube was saturated with NH_3 for 4 h. After cooling down to room temperature (5 K min^{-1}), the received product was washed in multiple steps with ethanol, water and acetone and dried under vacuum. Powder X-ray diffraction was conducted to confirm phase purity.

Synthesis of $Sr(N_3)_2$: $Sr(N_3)_2$ was synthesized starting from $SrCO_3$ (Sigma Aldrich, 99.995%) and HN_3 formed in situ (using aqueous NaN_3 (Acros Organics, 99%) and a cation exchanger (Amberlyst 15)) following the syntheses of Suhrmann and Karau.[43,44] HN_3 was slowly added to an aqueous suspension of $SrCO_3$ until the liquid turned clear. After filtration, the solution was evaporated under reduced pressure (50 mbar, 40 °C), recrystallized from acetone and dried under vacuum. FTIR and PXRD measurements were conducted to confirm phase purity. **Caution**: Since HN_3 solutions are potentially explosive and the vapour is highly poisonous, special care issues are necessary.

Ammonothermal synthesis: $Sr_3P_3N_7$ was synthesized under ammonothermal conditions starting from 0.5 mmol P_3N_5 (81.5 mg), 1.5 mmol SrH_2 (134.4 mg, Materion, 99.5%) and 5 mmol NaN_3 (325.0 mg, Sigma–Aldrich, 99.5%) as ammonobasic mineralizer. For the synthesis of Eu^{2+}-doped product 0.03 mmol $Eu(NH_2)_2$ (5.5 mg) was added to the reaction mixture. The starting materials were ground using an agate mortar and transferred into a Ta-liner, which protects the reaction mixture against autoclave impurities. The liner was placed in a high-temperature autoclave constructed of a nickel based super-alloy (Haynes® 282®, max. 1100 K, 170 MPa, 10 mL). The autoclave is sealed with a lid through flange joints using a silver coated Inconel® 718 ring (GFD seals). An Inconel® 718 high-pressure tube connects the lid with a hand valve (SITEC), which is equipped with a pressure transmitter (HBM P2VA1/5000 bar) and a bursting disc (SITEC). After evacuation, the sealed autoclave was cooled to 198 K using an ethanol/liquid nitrogen mixture and filled with NH_3 ($\approx$3.7 mL). A mass flow meter (D-6320-DR, Bronkhorst, Ruurlo, Netherlands) was used for detection of the amount of inserted ammonia. The filled autoclave was heated in two steps (heated to 670 K within 2 h, held at this temperature for 16 h, heated to 1070 K within 3 h and held at this temperature for 96 h) to 1070 K reaching a maximum pressure of 140 MPa. After cooling to room temperature and removal of NH_3, the reaction products were separated under argon, washed with ethanol and dried under vacuum. While the undoped product exhibits a white color, the Eu^{2+}-doped sample is orange.

High-pressure synthesis: Single crystals of $Sr_3P_3N_7$:Eu^{2+} were synthesized starting from stoichiometric amounts of $Sr(N_3)_2$ and P_3N_5 as well as small amounts of $EuCl_2$ (Strem Chemicals, 99.9%) as dopant using a modified Walker-type multianvil press.[24,25] The reactants were mixed and grounded in an agate mortar and packed in a capsule of hexagonal boron nitride (Henze, Kempten). After sealing with a BN-cap the sample was placed in the middle of a MgO octahedron (doped with 5% Cr_2O_3, edge length 18 mm, Ceramic Substrates & Components Ltd, Isle of Wight) using two MgO spacers (Cesima Ceramics, Wust-Fischbach). To ensure heating of the sample, the octahedron was further equipped with two graphite furnaces (Schunk Kohlenstofftechnik GmbH, Zolling), a ZrO_2 tube (Cesima Ceramics, Wust-Fischbach) for thermal insulation and two Mo plates for electrical contact between the graphite furnaces and the anvils of the multianvil press. The assembled octahedron was placed between eight WC cubes (doped with 7% Co, Hawedia, Marklkofen, Germany) with truncated edges (edge length 11 mm), which were separated with pyrophyllite gaskets (Ceramic Substrates & Components, Isle of Wight, UK). Further details on the experimental setup and the multianvil apparatus are given in the literature.[25] The sample was slowly compressed to 5 GPa and subsequently heated to 1270 K within 30 min. After 30 min at 1270 K the sample was allowed to cool down to room temperature within 30 minutes and slowly decompressed. The crystalline orange product was isolated and stored under argon.

Single-crystal X-ray diffraction: Single crystals of $Sr_3P_3N_7$:Eu^{2+} were placed and sealed in glass capillaries (Hilgenberg GmbH) in argon atmosphere for single-crystal XRD measurements. The data were collected using a Bruker D8 Quest diffractometer with $Mo_{K\alpha}$ radiation ($\lambda = 0.71073$ Å). The measured data were indexed and integrated with the software package APEX3.[45,46] APEX3 was also used for semi-empirical absorption corrections (SADABS) and the determination of the space group.[46–48] The crystal structure was solved using the SHELXT algorithm and refined by full-matrix least-squares methods using WinGX with implemented SHELXL.[49–51]

CCDC 1975990 contains the supplementary crystallographic data for this paper. These data are provided free of charge by The Cambridge Crystallographic Data Centrethrough the CCDC/FIZ Karlsruhe deposition service.

Powder X-ray diffraction: For powder XRD measurements, the ground product was filled and sealed in a glass capillary ($d=$ 0.3 mm, Hilgenberg GmbH). A Stoe STADI P diffractometer with $Cu_{K\alpha_1}$ ($\lambda=1.5406$ Å) radiation, Ge(111) monochromator and Mythen 1 K detector in modified Debye–Scherrer geometry was used for the measurements. TOPAS was used for Rietveld refinement of the data.[52]

Scanning electron microscopy: A scanning electron microscope (Dualbeam Helios Nanolab G3 UC (FEI), equipped with an EDX detector (X-Max 80 SDD, Oxford instruments)) was used for imaging of the crystals and for EDX measurements. Thereto, the crystallites were placed on adhesive carbon pads. A high-vacuum sputter coater (BAL-TEC MED 020, Bal Tec A) was used for coating of the samples with a conductive carbon film.

Fourier Transform Infrared (FTIR) spectroscopy: IR spectra (range between 400 and 4000 cm^{-1}) were collected using a FTIR-IFS 66 v/S spectrometer (Bruker). The samples were mixed with KBr (Acros Organics, 99%) and pressed into pellets under argon. OPUS was used for evaluation of the measurements.[53]

UV/Vis spectroscopy: The optical band gap was estimated using UV/Vis spectroscopy. For this purpose, diffuse reflectance measurements of the samples at room temperature were performed using a Jasco V-650 UV/VIS spectrophotometer equipped with Czerny–Turner mount, photomultiplier tube detector and deuterium (190–350 nm)/ halogen (330–900 nm) lamps as light sources.

Luminescence: A microcrystalline powder of $Sr_3P_3N_7:Eu^{2+}$ was used to determine luminescence properties. The measurement was conducted on a PTFE sample holder using an in-house built system based on a 5.3″ integration sphere and a spectrofluorimeter equipped with a 150 W Xe lamp, two 500 mm Czerny–Turner monochromators, 1800 1 mm^{-1} lattices, and 250/500 nm lamps, with a spectral range from 230 to 820 nm ($\lambda_{exc}=450$ nm). Additional data from a spectrometer sensitive in the 600–1100 nm wavelength range (Avantes) ($\lambda_{exc}=410$ nm) were used to obtain the complete emission band by merging data of both measurements. A comparison of integrated emission intensities and absorption at excitation wavelength ($\lambda_{exc}=438$ nm) of the sample with reference materials ($BaSO_4$, Merck for white standard DIN 5033 commercial $(Sr,Ca)AlSiN_3:Eu^{2+}$, Mitsubishi Chemical, and $Y_3Al_5O_{12}:Ce^{3+}$, Philips) were conducted to determine the internal quantum efficiency (IQE).

Acknowledgements

We acknowledge the Deutsche Forschungsgemeinschaft (DFG) for financial support within the research group „Chemistry and Technology of the Ammonothermal Synthesis of Nitrides“ (FOR 1600), project SCHN377/16-2. We also want to thank Arthur Haffner for single-crystal measurements, Marion Sokoll for FTIR measurements and Lisa Gamperl for EDX measurements (all at Department of Chemistry, LMU Munich) as well as the group of Prof. Dr. E. Schlücker for fabrication of the autoclaves (FAU Erlangen-Nürnberg).

Conflict of interest

The authors declare no conflict of interest.

Keywords: ammonothermal synthesis · crystal growth · high-pressure chemistry · luminescence · nitridophosphates

[1] S. D. Kloß, W. Schnick, *Angew. Chem. Int. Ed.* **2019**, *58*, 7933 – 7944; *Angew. Chem.* **2019**, *131*, 8015 – 8027.
[2] W. Schnick, J. Luecke, *J. Solid State Chem.* **1990**, *87*, 101 – 106.
[3] W. Schnick, V. Schultz-Coulon, *Angew. Chem. Int. Ed. Engl.* **1993**, *32*, 280 – 281; *Angew. Chem.* **1993**, *105*, 308 – 309.
[4] S. Wendl, W. Schnick, *Chem. Eur. J.* **2018**, *24*, 15889 – 15896.
[5] S. D. Kloß, W. Schnick, *Angew. Chem. Int. Ed.* **2015**, *54*, 11250 – 11253; *Angew. Chem.* **2015**, *127*, 11402 – 11405.
[6] F. J. Pucher, A. Marchuk, P. J. Schmidt, D. Wiechert, W. Schnick, *Chem. Eur. J.* **2015**, *21*, 6443 – 6448.
[7] A. Marchuk, W. Schnick, *Angew. Chem. Int. Ed.* **2015**, *54*, 2383 – 2387; *Angew. Chem.* **2015**, *127*, 2413 – 2417.
[8] A. Marchuk, S. Wendl, N. Imamovic, F. Tambornino, D. Wiechert, P. J. Schmidt, W. Schnick, *Chem. Mater.* **2015**, *27*, 6432 – 6441.
[9] S. Wendl, L. Eisenburger, M. Zipkat, D. Günther, J. P. Wright, P. J. Schmidt, O. Oeckler, W. Schnick, *Chem. Eur. J.* **2020**, *26*, 5010 – 5016.
[10] E. M. Bertschler, C. Dietrich, T. Leichtweiß, J. Janek, W. Schnick, *Chem. Eur. J.* **2018**, *24*, 196 – 205.
[11] W. Schnick, U. Berger, *Angew. Chem. Int. Ed. Engl.* **1991**, *30*, 830 – 831; *Angew. Chem.* **1991**, *103*, 857 – 858.
[12] A. Marchuk, F. J. Pucher, F. W. Karau, W. Schnick, *Angew. Chem. Int. Ed.* **2014**, *53*, 2469 – 2472; *Angew. Chem.* **2014**, *126*, 2501 – 2504.
[13] H. Jacobs, R. Nymwegen, *Z. Anorg. Allg. Chem.* **1997**, *623*, 429 – 433.
[14] M. Mallmann, S. Wendl, W. Schnick, *Chem. Eur. J.* **2020**, *26*, 2067 – 2072.
[15] M. Mallmann, C. Maak, R. Niklaus, W. Schnick, *Chem. Eur. J.* **2018**, *24*, 13963 – 13970.
[16] R. Dwiliński, A. Wysmolek, J. Baranowski, M. Kaminska, R. Doradziński, H. Jacobs, *Acta Phys. Pol. A* **1995**, *88*, 833 – 836.
[17] J. Hertrampf, P. Becker, M. Widenmeyer, A. Weidenkaff, E. Schlücker, R. Niewa, *Cryst. Growth Des.* **2018**, *18*, 2365 – 2369.
[18] J. Li, T. Watanabe, H. Wada, T. Setoyama, M. Yoshimura, *Chem. Mater.* **2007**, *19*, 3592 – 3594.
[19] T. Watanabe, K. Nonaka, J. Li, K. Kishida, M. Yoshimura, *J. Ceram. Soc. Jpn.* **2012**, *120*, 500 – 502.
[20] J. Häusler, L. Neudert, M. Mallmann, R. Niklaus, A.-C. L. Kimmel, N. S. A. Alt, E. Schlücker, O. Oeckler, W. Schnick, *Chem. Eur. J.* **2017**, *23*, 2583 – 2590.
[21] J. Häusler, S. Schimmel, P. Wellmann, W. Schnick, *Chem. Eur. J.* **2017**, *23*, 12275 – 12282.
[22] M. Mallmann, R. Niklaus, T. Rackl, M. Benz, T. G. Chau, D. Johrendt, J. Minár, W. Schnick, *Chem. Eur. J.* **2019**, *25*, 15887 – 15895.
[23] N. Cordes, R. Niklaus, W. Schnick, *Cryst. Growth Des.* **2019**, *19*, 3484 – 3490.
[24] D. Walker, *Am. Mineral.* **1991**, *76*, 1092 – 1100.
[25] H. Huppertz, *Z. Kristallogr.* **2004**, *219*, 330 – 338.
[26] H. Jacobs, U. Fink, *J. Less-Common Met.* **1979**, *63*, 273 – 286.
[27] H. Jacobs, S. Pollok, F. Golinski, *Z. Anorg. Allg. Chem.* **1994**, *620*, 1213 – 1218.
[28] F. Golinski, H. Jacobs, *Z. Anorg. Allg. Chem.* **1994**, *620*, 965 – 968.
[29] S. D. Kloß, N. Weidmann, R. Niklaus, W. Schnick, *Inorg. Chem.* **2016**, *55*, 9400 – 9409.
[30] V. Schultz-Coulon, W. Schnick, *Z. Anorg. Allg. Chem.* **1997**, *623*, 69 – 74.
[31] F. Liebau, *Structural Chemistry of Silicates*, Springer, Berlin, **1985**, 80.
[32] The terms *dreier* rings, *vierer* rings and *zweier* single chain were coined by Liebau and are derived from the German words „dreier, vierer and zweier“; a *dreier* ring comprises three tetrahedra centers, a *vierer* ring four tetrahedra centers, a *zweier* chain can be described as two polyhedra within one repeating unit of the linear part of the chain.
[33] E.-M. Bertschler, C. Dietrich, J. Janek, W. Schnick, *Chem. Eur. J.* **2017**, *23*, 2185 – 2191.

[34] F. W. Karau, L. Seyfarth, O. Oeckler, J. Senker, K. Landskron, W. Schnick, *Chem. Eur. J.* **2007**, *13*, 6841 – 6852.
[35] S. J. Sedlmaier, E. Mugnaioli, O. Oeckler, U. Kolb, W. Schnick, *Chem. Eur. J.* **2011**, *17*, 11258 – 11265.
[36] S. J. Sedlmaier, J. Schmedt auf der Günne, W. Schnick, *Dalton Trans.* **2009**, 4081 – 4084.
[37] R. López, R. Gómez, *J. Sol-Gel Sci. Technol.* **2012**, *61*, 1 – 7.
[38] J. Tauc, R. Grigorovici, A. Vancu, *Phys. Status Solidi B* **1966**, *15*, 627 – 637.
[39] L. M. Dale, A. Thewis, C. Boudry, I. Rotar, P. Dardenne, V. Baeten, J. A. F. Pierna, *Appl. Spectrosc. Rev.* **2013**, *48*, 142 – 159.
[40] A. A. Gowen, Y. Feng, E. Gaston, V. Valdramidis, *Talanta* **2015**, *137*, 43 – 54.
[41] M. Mallmann, J. Häusler, N. Cordes, W. Schnick, *Z. Anorg. Allg. Chem.* **2017**, *643*, 1956 – 1961.
[42] A. Stock, B. Hoffmann, *Ber. Dtsch. Chem. Ges.* **1903**, *36*, 314 – 319.
[43] R. Suhrmann, K. Clusius, *Z. Anorg. Allg. Chem.* **1926**, *152*, 52 – 58.
[44] F. W. Karau, *Dissertation*, Ludwig-Maximilians-Universität München (Germany) **2007**.
[45] *SAINT*, Data Integration Software, Madison, Wisconsin, USA, **1997**.
[46] *APEX 3*, Vers. 2016.2015-2010, Bruker-AXS, Karlsruhe, **2016**.
[47] G. M. Sheldrick, *SADABS*, *Multi-Scan Absorption Correction*, *v.2*, Bruker-AXS, Madison, WI, USA, **2012**.
[48] *XPREP Reciprocal Space Exploration*, Vers. 6.12, Bruker-AXS, Karlsruhe, **2001**.
[49] G. M. Sheldrick, *Acta Crystallogr. Sect. A* **2015**, *71*, 3 – 8.
[50] G. M. Sheldrick, *SHELXL-97: A program for crystal structure refinement*, University of Göttingen, Germany, **1997**.
[51] G. M. Sheldrick, *Acta Crystallogr. Sect. C* **2015**, *71*, 3 – 8.
[52] A. Coelho, *TOPAS Academic*, *Version 6*, Coelho Software, Brisbane (Australia), **2016**.
[53] *OPUS/IR*, Brucker Analytik GmbH, Karlsruhe, **2000**.

Manuscript received: January 18, 2020
Accepted manuscript online: February 7, 2020
Version of record online: April 28, 2020

